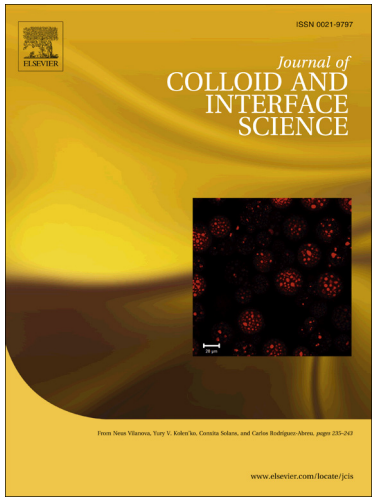

Gold nanoparticles-decorated silver-bipyridine nanobelts for the construction of mediatorless hydrogen peroxide biosensor

Abderrahmane Boujakhrout, Paula Díez, Alfredo Sánchez, Paloma Martínez-Ruíz, José M. Pingarrón, Reynaldo Villalonga

PII: S0021-9797(16)30541-0
DOI: http://dx.doi.org/10.1016/j.jcis.2016.07.074
Reference: YJCIS 21460

To appear in: *Journal of Colloid and Interface Science*

Received Date: 19 March 2016
Revised Date: 27 July 2016
Accepted Date: 28 July 2016

Please cite this article as: A. Boujakhrout, P. Díez, A. Sánchez, P. Martínez-Ruíz, J.M. Pingarrón, R. Villalonga, Gold nanoparticles-decorated silver-bipyridine nanobelts for the construction of mediatorless hydrogen peroxide biosensor, *Journal of Colloid and Interface Science* (2016), doi: http://dx.doi.org/10.1016/j.jcis.2016.07.074

GOLD NANOPARTICLES-DECORATED SILVER-BIPYRIDINE NANOBELTS FOR THE CONSTRUCTION OF MEDIATORLESS HYDROGEN PEROXIDE BIOSENSOR

Abderrahmane Boujakhrout,[a] *Paula Díez,**[a] *Alfredo Sánchez,*[a] *Paloma Martínez-Ruíz,*[b] *José M. Pingarrón,*[a] *Reynaldo Villalonga**[a]

[a]Department of Analytical Chemistry and [b]Department of Organic Chemistry I, Faculty of Chemistry, Complutense University of Madrid, 28040-Madrid Spain.

[*]Corresponding authors. Phone: +34 91 3944315, Fax: +34 91 3944329, E-mail: paula.diez@ucm.es, rvillalonga@quim.ucm.es

Abstract

Au nanoparticles modified with 4-mercaptopyridine and 6-mercapto-1-hexanol were used as coordination agents to prepare a novel hybrid nanomaterial with Ag:4,4´-bipyridine nanobelts. This nanohybrid was employed to modify glassy carbon electrodes and to construct a horseradish peroxidase-based mediatorless amperometric biosensor for H_2O_2. The electrode, poised at -100 mV, exhibited a rapid response within 4 s and a linear calibration range from 90 pM to 6.5 nM H_2O_2. The biosensor showed a high sensitivity of 283 A/M cm^2 and a very low detection limit of 45 pM at a signal-to-noise ratio of 3. The enzyme biosensor showed high stability when stored at 4ºC under dry conditions, retaining over 96% and 78% of its initial activity after 15 and 30 days of storage at 4ºC, respectively.

Keywords: Biosensor, gold nanoparticles, peroxidase, nanobelts, hydrogen peroxide.

1. Introduction

Electrochemical enzyme biosensors are widely employed as highly selective analytical tools for biomedical, food quality assurance, clinical diagnosis and environmental monitoring [1, 2]. In general, most of these biosensors devices need the use of electrochemical mediators to act as artificial electron transferring agents between the enzyme redox centre and the electrode surface. These mediators allow reduction of the overpotential and, accordingly, minimization of potential interferences during measurement [3, 4]. However, the use of electrochemical mediators implies somewhat complex electrode architectures, or even worse, the addition of these mediators to the measuring solution. Therefore, the design of novel nanostructured 3D transducer elements with improved electron transfer and electrocatalytic properties is a key factor to assemble simple, reliable and cost-effective third-generation enzyme biosensors.

Gold nanoparticles (AuNP) have been extensively employed in the preparation of electrochemical enzyme biosensors due to their unique characteristics such as high electroconductivity, surface energy and surface-to-volume ratio, electrocatalytic properties, ability to decrease proteins-metal particles distance, and the possibility to act as electroconductive wires between the electrode surface and the enzyme active site allowing direct electron transfer through a tunnelling mechanism [5]. In addition, tailor-made combination of AuNP with other micro- and nanosized materials has provided a large variety of advanced hybrid nanomaterials and nanocomposites with new and synergic properties for biosensing purposes [6-8].

AuNP have been directly employed as transducer elements in enzyme biosensor by modification of the electrode surface via covalent attachment, electrodeposition, electrostatic adsorption, electropolymerization or supramolecular association [9-12]. On the other hand, a great variety of functional biosensor interfaces has been designed by combining gold nanoparticles with carbon nanotubes [6, 13], graphene derivatives [14, 15], electroconductive polymers [7], dendrimers [16], metal and metal oxide nanostructures [12, 17, 18], polysaccharides [19], etc.

In this work we describe the synthesis of original bi-functionalized AuNP capped with 4-mercaptopyridine and 6-mercapto-1-hexanol residues, and its further use to prepare novel AuNP-decorated coordination polymer nanobelts by reaction with 4,4´-bipyridine and Ag^+ ions. This nanohybrid was successfully employed as wiring material for horseradish peroxidase (HRP, EC 1.11.1.7) to construct a highly sensitive mediatorless enzyme biosensor for hydrogen peroxide. The rational of this research is supported by the well-known electrocatalytic properties of AuNP [20, 21] and silver:bipyridine coordination polymers-based nanostructures [22], allowing us to envision a synergic electrocatalytic capacity for the resulting nanohybrid.

On the other hand, hydrogen peroxide was selected as target analyte due to its function as essential mediator in biology, medicine and chemistry, as well as its environmental impact as industrial waste. In addition, H_2O_2 is a by-product of highly selective oxidases commonly employed in enzyme biosensor design [23].

2. Materials and Methods

2.1. Reagents and apparatus

Horseradish peroxidase (HRP, Type II, 10^5 U/mg), $HAuCl_4$, $NaBH_4$, $AgNO_3$, 4-mercaptopyridine, 6-mercapto-1-hexanol and 4,4´-bipyridine were purchased from Sigma (USA). All other chemicals were of analytical grade.

Transmission electron microscopy (TEM) and high resolution field emission scanning electron microscopy (FE-SEM) were performed with JEOL JEM 2100 and JEOL JSM-6335F microscopes, respectively (JEOL Ltd., Japan). X-ray photoelectron spectroscopy (XPS) analysis was performed with a SPECS GmbH electron spectroscopy system provided with a PHOIBOS 150 9MCD analyser. Amperometric measurements were performed with an Inbea potentiostat (Inbea Biosensores S.L., Spain). Cyclic voltammetry (CV) and electrochemical impedance spectroscopy (EIS) experiments were performed using a FRA2 µAutolab Type III potentiostat/galvanostat (Metrohm Autolab B.V., The Netherlands). A conventional three-electrode system was employed in the electrochemical

studies, where the working electrode was a glassy carbon electrode (GCE, 3.0 mm diameter) modified with the nanobelts and the immobilized enzyme. An Ag/AgCl/KCl (3 M) and a Pt wire were used as reference and counter electrodes, respectively. The measurements with the biosensor were carried out at 25ºC in 0.1 M sodium phosphate buffer, pH 6.0 (working volume 10 ml). The solution was exhaustively de-aerated before each electrochemical experiment. The solutions were stirred at 300 rpm with a magnetic bar during amperometric measurements. For analytical purposes, 1 µM H_2O_2 solutions in 50 mM sodium phosphate buffer, pH 6.0 were freshly prepared.

2.2. Synthesis of the functionalized AuNP

Bi-functionalized AuNP were prepared through a modification of our previously reported protocol [6, 10]. Briefly, 50 mg of $HAuCl_4$ were dissolved in 12.7 mL of de-aerated DMSO. This solution was added dropwise to other 12.7 mL of de-aerated DMSO containing 60 mg sodium borohydride, 10 mg 4-mercaptopyridine and 36.2 mg 6-mercapto-1-hexanol under vigorous stirring. The reaction mixture turned deep brown immediately, but the reaction was continued for 24 h. The functionalized AuNPs were then precipitated by adding 25 mL CH_3CN, collected by centrifugation, and washed with 50 mL CH_3CN:DMSO (1:1 v/v), 50 mL ethanol and 10 mL diethyl ether. The nanoparticles were finally isolated by centrifugation and dried under N_2.

2.3. Preparation of the AuNP-NB hybrid nanomaterial

This hybrid nanomaterial was prepared by modification of the protocol reported for silver:bipyridine nanobelts [22]. Stock solutions of 10 mg/mL AuNP and 34 mg/mL $AgNO_3$ in double distilled water, and 13 mg/mL 4,4´-bipyridine in ethanol were freshly prepared. To prepare the AuNP-NB nanohybrid, 200 µL of AuNP solution were mixed with 1 mL $AgNO_3$ and 2 mL 4,4´-bipyridine stock solution under continuous stirring at room temperature. After 10 min, the resulting purple precipitate was centrifuged, two-times washed with ethanol and finally dispersed in ethanol up to 14 mg/mL final concentration.

2.4. Preparation of the nanostructured enzyme electrode

A polished GCE was first coated with the nanohybrid material by depositing 20 µL of the AuNP-NB ethanolic dispersion on the electrode surface and allowing drying. HRP was further immobilized on the nanostructured electrode by dropping 12 µL of a 10 mg/mL enzyme solution in 100 mM sodium phosphate buffer, pH 6.0, and mixed with 2 µL of 25% (v/v) glutaraldehyde. The electrode was kept at 4ºC for 1 h, then washed several times with cold 50 mM sodium phosphate buffer, pH 6.0, dried and finally stored in refrigerator until use (HRP/AuNP-NB/GCE).

3. Results and Discussion

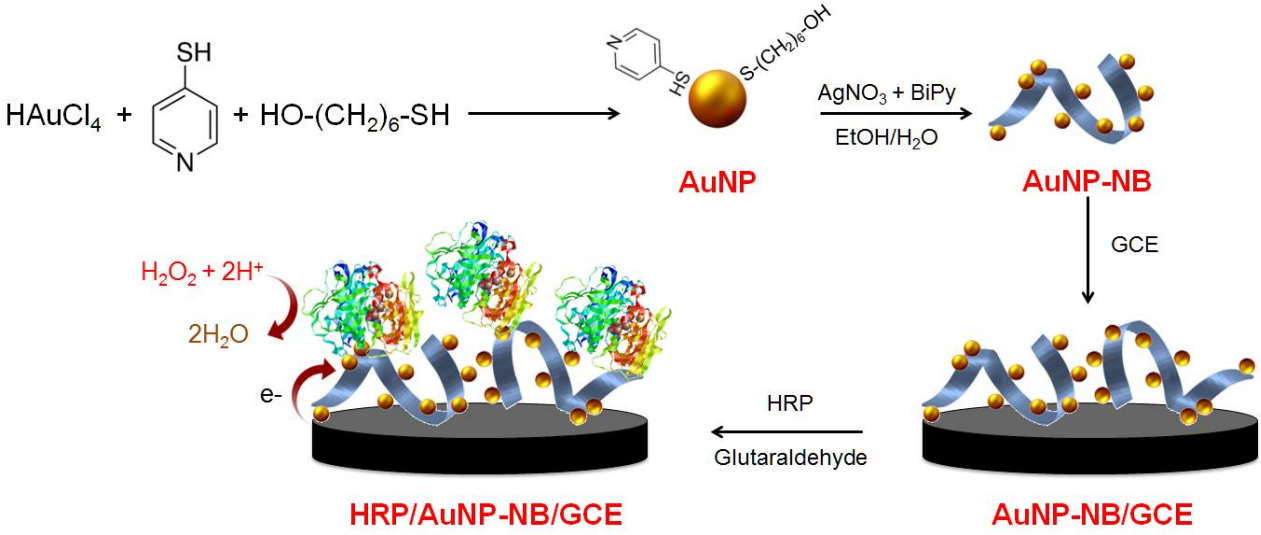

Scheme 1. Schematic display of the processes involved in the preparation of the AuNP-NB nanohybrid and assembly of the HRP enzyme biosensor.

The steps involved in the preparation of the hybrid nanomaterial and the HRP enzyme electrode is illustrated in Scheme 1. Gold colloids were first grown in the presence of two different thiol ligands, 4-mercaptopyridine and 6-mercapto-1-hexanol, yielding dark red and water soluble nanoparticles. The bi-functionalized AuNP particles showed spherical geometry with an average diameter of 2.7 ± 0.9 nm, as determined by TEM (Figure 1A). The radial geometry and small size exhibited by the nanoparticles resulted from the synthetic approach used, in which both metal reduction and

attachment of thiolated ligands to the surface of the developing Au particles take place in the same step [10, 24]. The size histogram for the AuNPs is reported in Figure 1S (Supporting Information).

The selection of the two different thiol-derivatives used as capping ligands for the AuNPs was rational made according to the desired properties to be conferred to the nanomaterial. In this sense, 4-mercaptopyridine acted as chelating agent able to coordinate silver ions, and accordingly, allowing the coordination of functionalized the AuNP to the silver:bipyridine nanobelts. On the other hand, 6-mercapto-1-hexanol should favour the solubilisation and colloidal stabilization of the resulting nanoparticles in aqueous solutions.

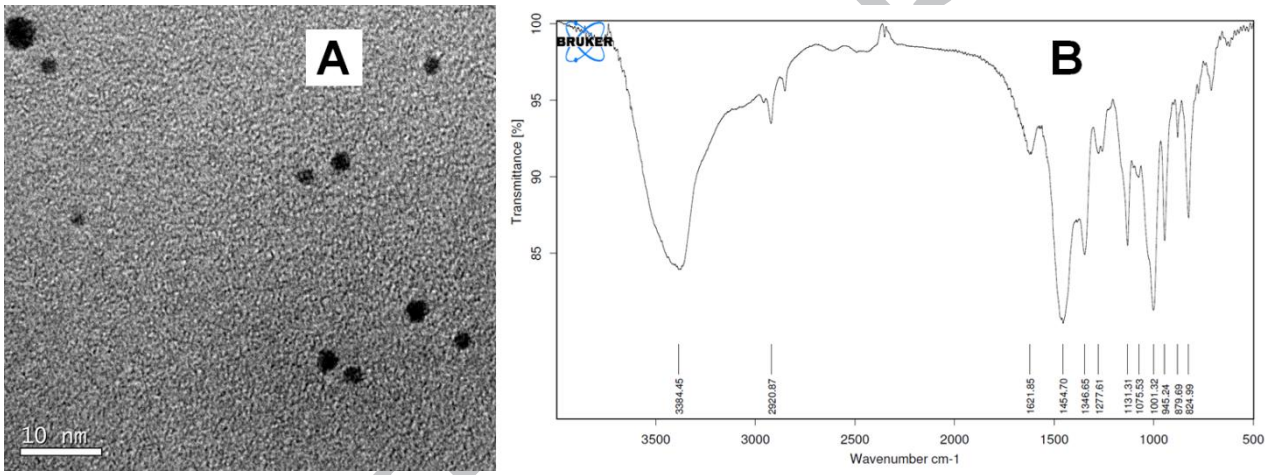

Figure 1. TEM (A) and FT-IR (B) analysis of bi-functionalized Au nanoparticles.

Bi-functionalized AuNP were characterized by FT-IR (Figure 1B). The presence of 4-mercaptopyridine was confirmed by the peaks at 16254.85 cm^{-1}, 14554.70 cm^{-1} and 13476.64 cm^{-1}, corresponding to the symmetric wag-stretch, symmetric C-H wag and C-H wag in the aromatic pyridine ring, respectively. In addition, the presence 6-mercapto-1-hexanol was verified by the broad peak centered at 3384.45 cm^{-1} due to the stretching of the O-H groups, the peak at 29210.87 cm^{-1} corresponding to the stretching of the C-H groups, and the C-O stretching peak at 1001.32 cm^{-1}.

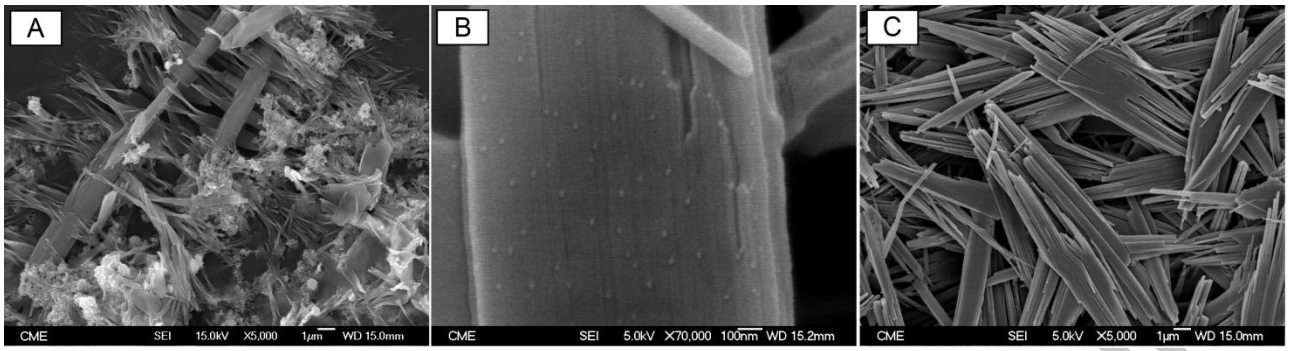

Figure 2. Representative FE-SEM images of AuNP-NB nanohybrid at low (A) and high (B) magnification, and non-decorated silver:bipyridine nanobelts (C).

Functionalized AuNP were mixed with $AgNO_3$ and 4,4´-bipyridine, yielding a purple solid that can be easily suspended in ethanol. FE-SEM analysis revealed a fractal-like dendritic morphology for this nanomaterial, which was noticeably enriched with AuNP (Figure 2A). Although bulky grouped nanoparticles were clearly observed, FE-SEM images at high magnification revealed that nanoparticles were attached to the nanobelt surface (Figure 2B). This fact suggested partial coordination of functionalized AuNP to the silver:bipyridine nanobelts structure through bipyridine:silver:bipyridine linkages, and further formation of AuNP coordination adducts on this decoration sites. The effect of AuNP on the morphology of the decorated nanobelts can be easily visualized by comparison with FE-SEM image of non-doped silver:bipyridine coordination polymers (Figure 2C), which showed the classical non-dendritic nanobelt morphology [22].

These results were confirmed by TEM analysis, as is illustrated in Figure 3. In contrast with non-doped nanostructures, which showed well-defined nanobelt morphology, AuNP-NB nanohybrid showed interesting fern-like fractal morphology with an average size of 11 ± 4 µm. TEM images at high magnification revealed a high content of AuNP homogeneously distributed into the nanohybrid structure. The size histogram for the AuNPs is reported in Figure 1S (Supporting Information).

Z-potential analysis in milliQ water revealed values of +14.2 mV and +6.6 mV for non-doped silver:bipyridine coordination polymers and AuNP-NB nanohybrids, respectively.

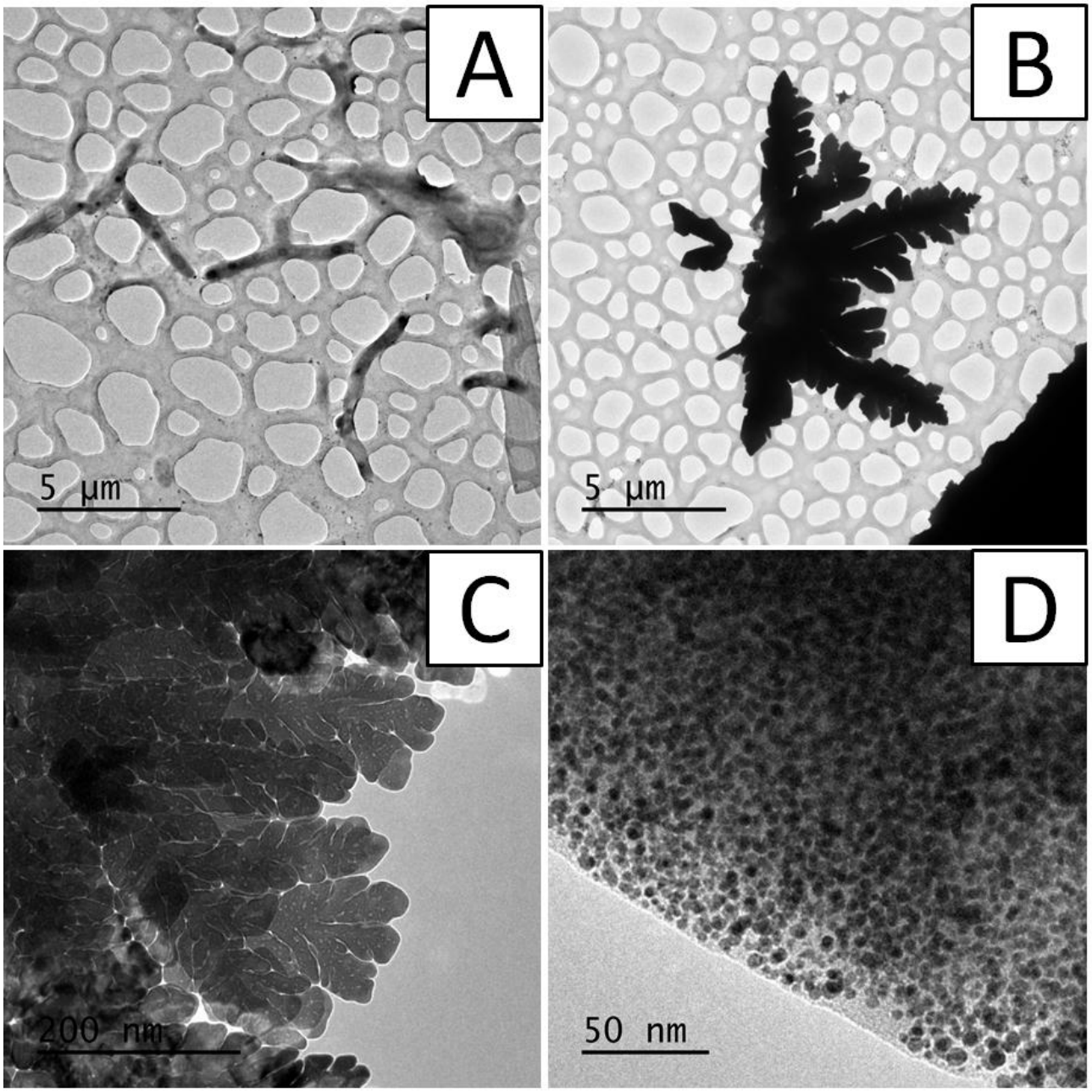

Figure 3. Representative TEM images of non-decorated silver:bipyridine nanobelts (A) and AuNP-NB nanohybrid at different magnification (B-D).

The nanomaterials were characterized by XPS, and the corresponding spectra are shown in Figures 2S-4S (Supporting Information). Polyfunctionalized AuNPs showed the characteristics peaks of Au^0: the 4*f* doublet at 84.1 eV ($4f_{7/2}$) and 87.7 eV ($4f_{5/2}$), the 4*d* doublet at 368.2 eV ($4d_{5/2}$) and 374.1 eV ($4d_{3/2}$) and the component $4p_{3/2}$ at 532.4 eV of the 4*p* doublet (Figure 2S). On the other hand, the XPS spectrum of silver:bipyridine nanobelts in Figure 3S is mainly characterized by the

prominent 3*d* doublet at 371.4 eV ($3f_{5/2}$) and 377.3 eV ($3f_{3/2}$) of Ag^{+}. These peaks are also clearly observed in the XPS spectrum of AuNP-NB (Figure 4S), which were slightly shifted to 370.9 eV ($3f_{5/2}$) and 376.8 eV ($3f_{3/2}$) due to interaction with the chelating groups at the surface AuNPs. The presence of AuNPs in the nanohybrid was confirmed by the peaks at 87.3 eV ($4f_{7/2}$) and 90.9 eV ($4f_{5/2}$). This shifting in the 4*d* doublet suggests high perturbation of electrons at the AuNP surface, which could be caused by the proximity of silver ions attached to the mercaptopyridine residues.

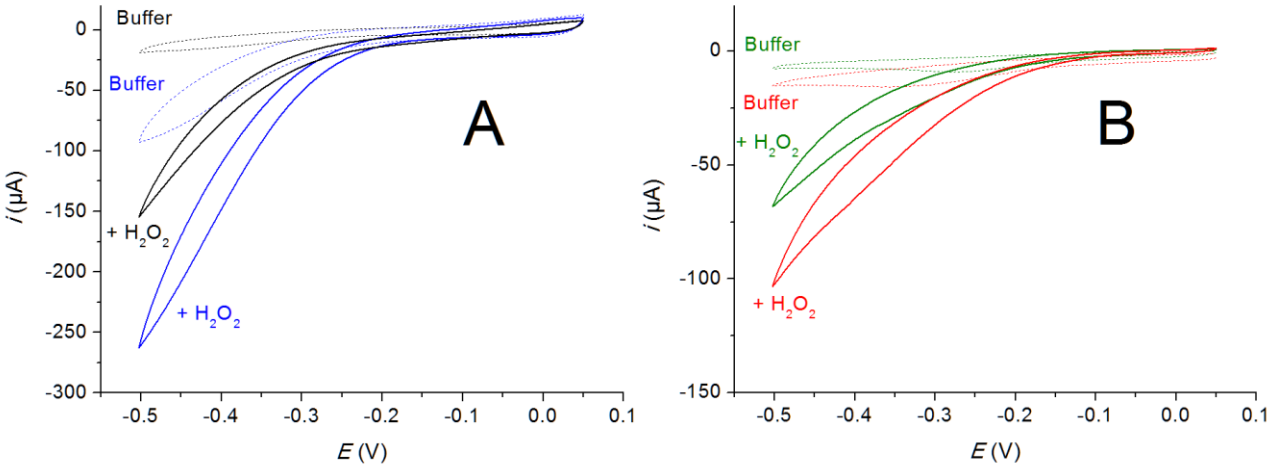

Figure 4. Cyclic voltammograms recorded at the HRP/AuNP-NB/GCE (blue lines), AuNP-NB/GCE (black lines), NB/GCE (green lines) and HRP/NB/GCE (red lines) in 0.1 M sodium phosphate buffer, pH 6.0 at scan rate of 50 mV/s before (dotted lines) and after (solid lines) 3 nM H_2O_2 additions.

The hybrid nanomaterial was used to modify a GCE, on which HRP was covalently immobilized through a glutaraldehyde-mediated cross-linking reaction. The behaviour of the resulting enzyme electrode (HRP/AuNP-NB/GCE) was evaluated by cyclic voltammetry using H_2O_2 as substrate. As controls, GCE coated with AuNP-NB, AuNP, HRP/AuNP, NB and HRP/NB were also prepared. Figure 4A compares cyclic voltammograms recorded at the HRP/AuNP-NB/GCE and AuNP-NB/GCE electrodes in a deaerated 0.1 M sodium phosphate buffer solution of pH 6.0 at a 50 mV/s scan rate, in the absence and the presence of added H_2O_2. Similar study is shown in Figure 5S

(Supporting Information) for the AuNP/GCE and HRP/AuNP/GCE electrodes. No redox peaks were observed in the voltammograms recorded with the AuNP/GCE, NB/GCE and AuNP-NB/GCE, suggesting these nanomaterials were not electrochemically transformed under these conditions. A noticeable increase in the cathodic current was observed for the AuNP-NB/GCE control electrode after addition of H_2O_2 (black lines). This effect was significantly higher than that observed at a GCE only coated with silver:bipyridine NB (Figure 4B, green lines, please note the different current scale) or AuNPs (Figure 5S, Supporting Information). This fact clearly indicated the high electrocatalytic ability of the synthesized nanohybrid for the electrochemical reduction of H_2O_2 at the nanostructured electrode surface.

As expected, remarkably larger catalytic currents were found at the HRP/AuNP-NB/GCE electrode after addition of H_2O_2 (Figure 3A, blue lines), which were also higher than those observed with the HRP/NB/GCE electrode (Figure 3B, red lines), and the HRP/AuNP/GCE electrode (Figure 5S, Supporting Information). These results demonstrated that the electrocatalytic behaviour of HRP was improved upon its immobilization on the AuNP-NB nanohybrid, allowing an efficient electron transfer between the redox active site of the enzyme and the electrode surface.

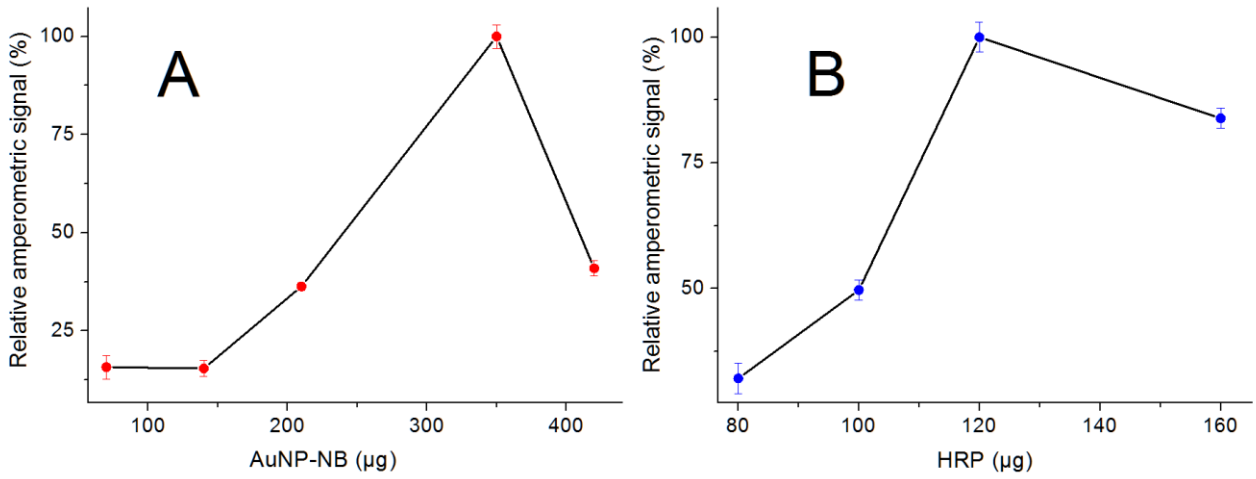

Figure 5. Influence of the AuNP-NB (A) and HRP (B) loadings on the amperometric signal recorded with the HRP/AuNP-NB/GCE enzyme biosensors after addition of 10 µL of 1.0 µM H_2O_2 in 0.1 M sodium phosphate buffer, pH 6.0. Working potential = -100 mV.

To construct an amperometric enzyme biosensor for the mediatorless detection of H_2O_2, the parameters involved in the assembly of the HRP-based electrode were optimized by measuring the amperometric responses recorded at -100 mV toward additions of 1 µM H_2O_2. Figure 5 shows as the measured current increased with the AuNP-NB hybrid nanomaterial loading up to 350 µg. High AuNP-NB loading caused a reduction in the analytical signal, which can be ascribed to low mechanical stability of the nanostructured film, thus leaking from the electrode surface. Moreover, covalent immobilization of 120 µg HRP provided also the larger amperometric responses and, therefore, the enzyme electrodes were assembled using these optimal conditions.

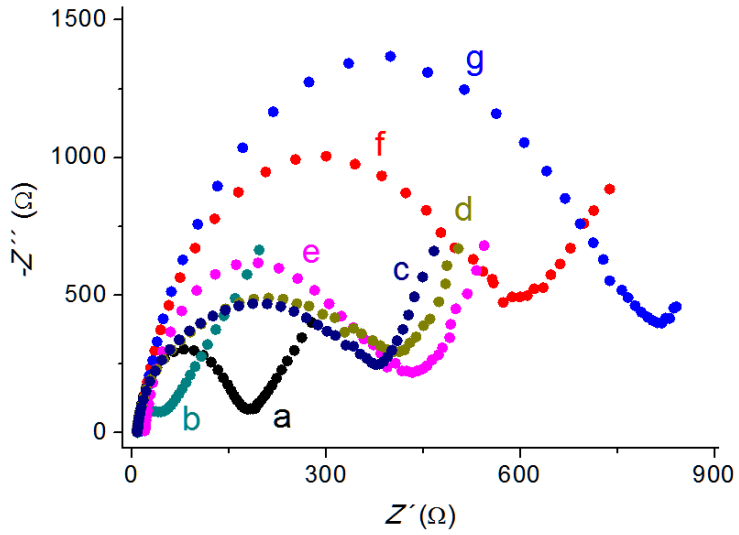

Figure 6. Nyquist plots of bare GCE (a), AuNP/GCE (b), HRP/AuNP/GCE (c), NB/GCE (d), HRP/NB/GCE (e), AuNP-NB/GCE (f) and HRP/AuNP-NB/GCE (g) in 0.1 M KCl solution containing 5 mM $K_3[Fe(CN)_6]/K_4[Fe(CN)_6]$ (1:1).

The assembly of the enzyme electrode under the optimized conditions was studied by electrochemical impedance spectroscopy using $[Fe(CN)_6]^{4-/3-}$ ions as redox probe. The corresponding Nyquist plots are shown in Figure 6. Coating of bare GCE with the AuNP-NB caused an increase in the electron transfer resistance, which could be ascribed to the less conductive

properties of the hybrid material. In addition, a noticeable increase in the electron transfer resistance was observed upon HRP immobilization, indicating high enzyme loading on the modified electrode surface. Similar impedance behaviour was observed for control electrodes prepared by coating GCE with AuNPs and silver:bipyridine nanobelts (NB) and further immobilization of HRP, suggesting these nanomaterials also favour high protein loading upon immobilization.

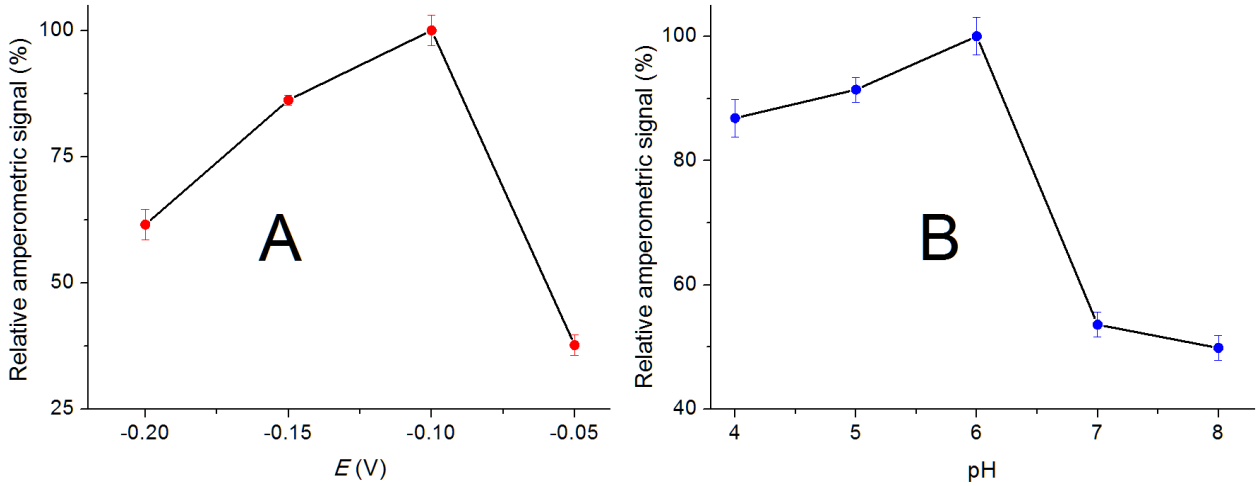

Figure 7. Influence of working potential (A, pH 6.0) and pH (B, *E* = -100 mV) on the amperometric signal recorded with the HRP/AuNP-NB/GCE biosensor after addition of 10 µL of 1.0 µM H_2O_2 in 0.1 M sodium phosphate buffers.

The nanostructured electrode was further employed to construct a mediatorless amperometric biosensor for H_2O_2. Optimal working conditions for this biosensor were determined by evaluating the influence of the applied potential and pH on the amperometric response of the enzyme electrode towards addition of 1.0 µM H_2O_2. As it can be seen in Figure 7, higher currents were measured when the working potential was fixed at -100 mV versus Ag/AgCl and analytical determinations were performed in pH 6.0 solutions.

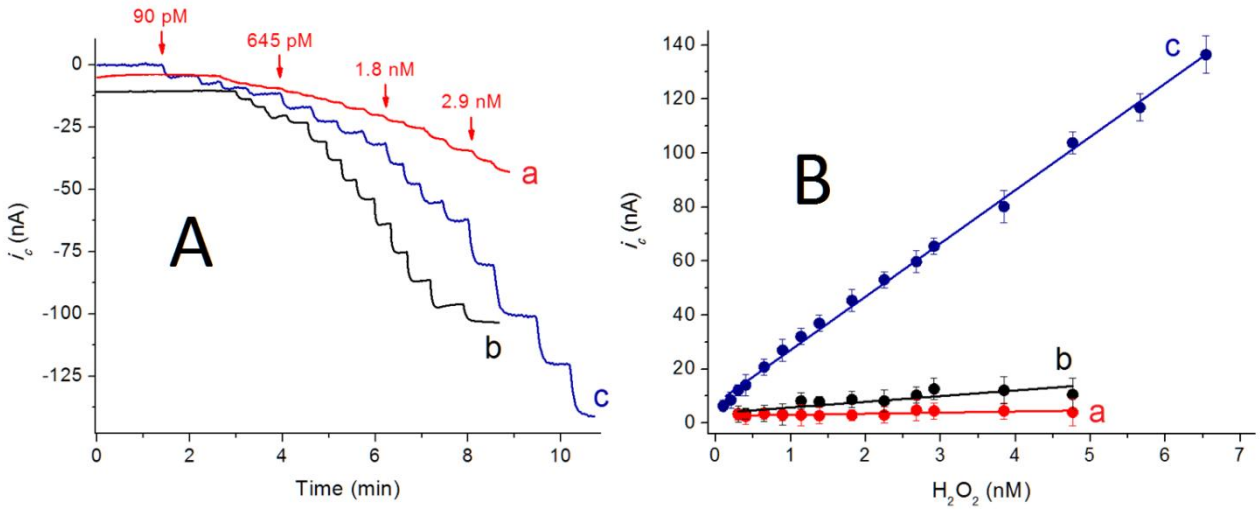

Figure 8. Amperometric responses (A) and calibration curve (B) recorded with the HRP/NB/GCE (a), HRP/AuNP/GCE (b) and HRP/AuNP-NB/GCE (c) biosensors toward H_2O_2. E_{app} = -100 mV, stirring condition: 300 rpm.

The amperometric responses obtained with the HRP/AuNP-NB/GCE electrode to successive additions of H_2O_2 are shown in Figure 8A. As controls, HRP/AuNP/GCE and HRP/NB/GCE electrodes were also tested. The mediatorless biosensor exhibited a very fast response to H_2O_2, reaching about 95% of the steady-state signals within 4 seconds. This amperometric biosensor was able to detect H_2O_2 at very low concentration, exhibiting a linear range of response (r = 0.998, n = 10) between 90 pM and 6.5 nM, according to the following equation:

$$i_c(\mathrm{A}) = 17.7 \times c(H_2O_2/\mathrm{M}) + 9 \cdot 10^{-9}$$

The biosensor showed a high sensitivity of 283 A/M cm^2 (17.7 A/M) and a very low detection limit of 45 pM at a signal-to-noise ratio of 3. It should be noticed that the control electrodes also showed electroanalytical response toward H_2O_2. However, their analytical behaviour was lower in comparison with the HRP/AuNP-NB/GCE based biosensor in term of linear range of response, sensitivity and limit of detection.

In comparison with other AuNP-based electrochemical biosensors previously described in literature, the HRP/AuNP-NB/GCE electrode showed best analytical characteristics in terms of linear range of

response and limit of detection (Table 1). In addition, the biosensor showed higher sensitivity than those based on recombinant HRP adsorbed on polycrystalline gold (1.4 A/M cm^2) [25], HRP immobilized on electropolymerized gold nanoparticles (498 μA/M cm^2) [10], HRP attached to ferrocene-modified chitosan (28.4 nA/M) [26] and HRP immobilized on carbon nanodots/CoFe layered double hydroxides (55 mA/M cm^2) [27].

Table 1. Comparison of analytical properties of the biosensor with previously reported AuNP-based H_2O_2 biosensors

Electrode	E (mV)	Linear Range (mM)	Detection Limit (μM)	Sensitivity (A/M cm^2)	Reference
HRP/polyAuNP/Au	0	$5\cdot10^{-3}$ - 1.1	$1.5\cdot10^{-6}$	$4.9\cdot10^{-4}$	[10]
HRP/pcAu	-50	$1\cdot10^{-7}$ - $4.0\cdot10^{-5}$	$1.0\cdot10^{-8}$	1.4	[25]
HRP/C-Dots/LDHs/GCE	-350	$1\cdot10^{-4}$ - $2.3\cdot10^{-2}$	0.04 μM	$5.5\cdot10^{-2}$	[27]
HRP/ZnO-AuNP-Naf/GCE	-300	0.015 - 1.1	$9\cdot10^{-6}$	-	[28]
HRP/AuNP/Gph/Chi/GCE	-300	$5\cdot10^{-3}$ - 5.13	$1.7\cdot10^{-6}$	-	[29]
HRP/$CaCO_3$-AuNP/Au	-200	$5\cdot10^{-4}$ - 5.2	$1\cdot10^{-7}$	-	[30]
HRP/AuNP-SF/GCE	-600	0.01 - 1.8	$5\cdot10^{-6}$	-	[31]
HRP-AuNP/ALG/Au	-400	0.02 - 13.7	$3\cdot10^{-6}$	$4.0\cdot10^{-2}$	[32]
HRP/AuNP/ITO	-150	$8\cdot10^{-3}$ - 3.0	$2\cdot10^{-6}$	-	[33]
HRP/AuNP-NB/GCE	-100	$9\cdot10^{-8}$ - $6.5\cdot10^{-6}$	$4.5\cdot10^{-11}$	283	This work

AuNP: Gold nanoparticles; Naf: Nafion; Gph: graphene; Chi: chitosan; SF: silk fibroin; ALG: sodium alginate; ITO: indium tin oxide electrode, pcAu: polycrystalline Au electrode; C-Dots: carbon nanodots; LDHs: CoFe layered double hydroxides.

The reproducibility of the enzyme biosensor was estimated by measuring the response of five different electrodes to 1 nM H_2O_2, and the relative standard deviation for these measurements was

calculated as 7.4%. In addition, a relative standard deviation of 4.9% was calculated when the same electrode was used to measure repeatedly ten different 100 pM H_2O_2 additions.

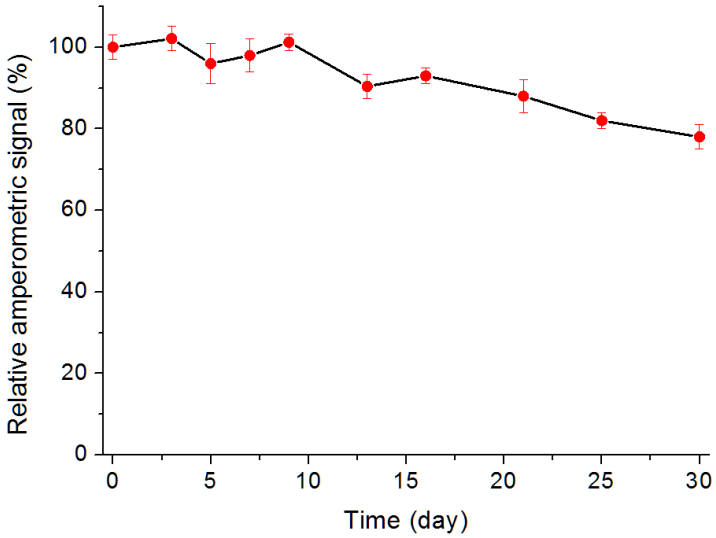

Figure 9. Effect of time of storage at 4ºC on the amperometric responses of the biosensor.

Figure 9 shows the effect of time of storage at 4ºC under dry conditions on the amperometric response of the biosensor toward 2 nM H_2O_2. The reagentless biosensor exhibited good storage stability, retaining 96% and 78% of its initial activity after 15 and 30 days of storage at 4ºC, respectively. On the other hand, the biosensor showed excellent selectivity toward H_2O_2, with no significant changes in the amperometric response toward 2 nM H_2O_2 in the presence of L-glucose, ethanol, acetic acid, sucrose, lactic acid, uric acid and citric acid at 1 µM concentration. Under these conditions, the biosensor only showed a little change of about 7% in the amperometric response after addition of 1 µM ascorbic acid.

Conclusions

A novel hybrid nanomaterial based on silver:bipyridine nanobelts decorated with bi-functionalized AuNP was prepared. In contrast to previously reported non-doped nanomaterial [22], this nanohybrid showed interesting fern-like fractal morphology. The electrocatalytic activity toward H_2O_2 was also noticeably improved, and accordingly, this new nanohybrid was employed to

construct a mediatorless enzyme biosensor able to detect the analyte at picomolar levels. The biosensor exhibited a superior analytical performance than other previously described [25-33], in terms of sensitivity, selectivity, stability, fast electroanalytical response and limit of detection. According to our results, it can be predicted that this nanohybrid could be employed as electroactive transduction element for the assembly of other advanced amperometric enzyme biosensors.

Acknowledgements

Financial support from the Spanish Ministry of Economy and Competitiveness CTQ2014-58989-P, CTQ2015-71936-REDT, CTQ2015-64402-C2-1-R and Comunidad de Madrid S2013/MIT-3029, Programme NANOAVANSENS is gratefully acknowledged.

References

[1] N.J. Ronkainen, H.B. Halsall, W.R. Heineman, *Chem. Soc. Rev.* **39** (2010) 1747-1763.

[2] K. Kerman, M. Saito, E. Tamiya, S. Yamamura, Y. Takamura, *Trends Anal. Chem.* **27** (2008) 585-592.

[3] M. Zhang, W. Gorski, *Anal. Chem.* **77** (2005) 3960-3965.

[4] A. Chaubey, B.D. Malhotra, *Biosens. Bioelectron.* **17** (2002) 441-456.

[5] S. Bharathi, M. Nogami, S. Ikeda, *Langmuir* 17 (2001) 1-4.

[6] R. Villalonga, P. Díez, M. Eguílaz, P. Martínez, J.M. Pingarrón, *ACS Appl. Mater. Interfaces* **4** (2012) 4312-4319.

[7] N. German, A. Kausaite-Minkstimiene, A. Ramanavicius, T. Semashko, R. Mikhailova, A. Ramanaviciene, *Electrochim. Acta* **169** (2015) 326-333.

[8] H. Ekram, A. Galal, N.F. Atta, *J. Electroanal. Chem.* **749** (2015) 42-52.

[9] Y. Yang, A.M. Asiri, D. Du, Y. Lin, *Analyst* **139** (2014) 3055-3060.

[10] R. Villalonga, P. Díez, P. Yáñez-Sedeño, J.M. Pingarrón, *Electrochim. Acta* **56** (2011) 4672-4677.

[11] X. Cai, X. Gao, L. Wang, Q. Wu, X. Lin, *Sens. Actuator B Chem.* **181** (2013) 575-583.

[12] X. Liu, J. Zhang, S. Liu, Q. Zhang, X. Liu, D.K. Wong, *Anal. Chem.* **85** (2013) 4350-4356.

[13] M. Eguílaz, R. Villalonga, J.M. Pingarrón, N.F. Ferreyra, G.A. Rivas, *Sens. Actuator B Chem.* 216 (2015) 629-637.

[14] S. Azzouzi, L. Rotariu, A.M. Benito, W.K. Maser, M.B. Ali, C. Bala, *Biosens. Bioelectron.* **69** (2015) 280-286.

[15] S. Abraham, N.R. Nirala, S. Pandey, M. Srivastava, S. Srivastava, B. Walkenfort, A. Srivastava, *Anal. Met.* **7** (2015) 3993-4002.

[16] Z.M. Liu, Y. Yang, H. Wang, Y.L. Liu, G.L. Shen, R.Q. Yu, *Sens. Actuator B Chem.* **106** (2005) 394-400.

[17] Y. Zhao, X. Fang, X. Yan, X. Zhang, Z. Kang, G. Zhang, Y. Zhang, *Microchim. Acta* **182** (2015) 605-610.

[18] A. Boujakhrout, E. Sánchez, P. Díez, A. Sánchez, P. Martínez-Ruiz, C. Parrado, J.M. Pingarrón, R. Villalonga, *ChemElectroChem* **2** (2015) 1735-1741.

[19] R. Villalonga, R. Cao, J. Hernández, C. Camacho, *Chem. Commun.* (2007) 942-944.

[20] H.G. Liao, Y.X. Jiang, Z.Y. Zhou, S.P. Chen, S.G. Sun, *Angew. Chem.* **120** (2008) 9240-9243.

[21] M.C. Daniel, D. Astruc, *Chem. Rev.* **104** (2004) 293-346.

[22] Y. Luo, W. Lu, G. Chang, F. Liao, X. Sun, *Electrochim. Acta* **56** (2011) 8371-8374.

[23] C. Camacho, J.C. Matías, B. Chico, R. Cao, L. Gómez, B.K. Simpson, R. Villalonga, *Electroanalysis* **19** (2007) 2538-2542.

[24] J. Liu, W. Ong, E. Román, M.J. Lynn, A.E. Kaifer, *Langmuir* **16** (2000) 3000-3002.

[25] E.E. Ferapontova, V.G. Grigorenko, A.M. Egorov, T. Börchers, T. Ruzgas, L. Gorton, *Biosens. Bioelectron.* **16** (2001) 147-157.

[26] A. Garcia, C. Peniche-Covas, B. Chico, B.K. Simpson, R. Villalonga, *Macromol. Biosci.* **7** (2007) 435-439.

[27] Y. Wang, Z. Wang, Y. Rui, M. Li, *Biosens. Bioelectron.* **64** (2015) 57-62.

[28] C. Xiang, Y. Zou, L.X. Sun, F. Xu, *Sens. Actuator B Chem.* **136** (2009) 158-162.

[29] K.F. Zhou, Y.H. Zhu, X.L. Yang, J. Luo, C.Z. Li, S.R. Luan, *Electrochim. Acta* **55** (2010) 3055-3060.

[30] F. Li, Y. Feng, Z. Wang, L.M. Yang, L.H. Zhuo, B. Tang, *Biosens. Bioelectron.* **25** (2010) 2244-2248.

[31] H. Yin, S. Ai, W. Shi, L. Zhu, *Sens. Actuator B Chem.* **137** (2009) 747-753.

[32] B. Chico, C. Camacho, M. Pérez, M.A. Longo, M.A. Sanromán, J.M. Pingarrón, R. Villalonga, *J. Electroanal. Chem.* **629** (2009) 126-132.

[33] J. Wang, L. Wang, J. Di, Y. Tu, *Talanta* **77** (2009) 1454-1459.

*3: Graphical Abstract

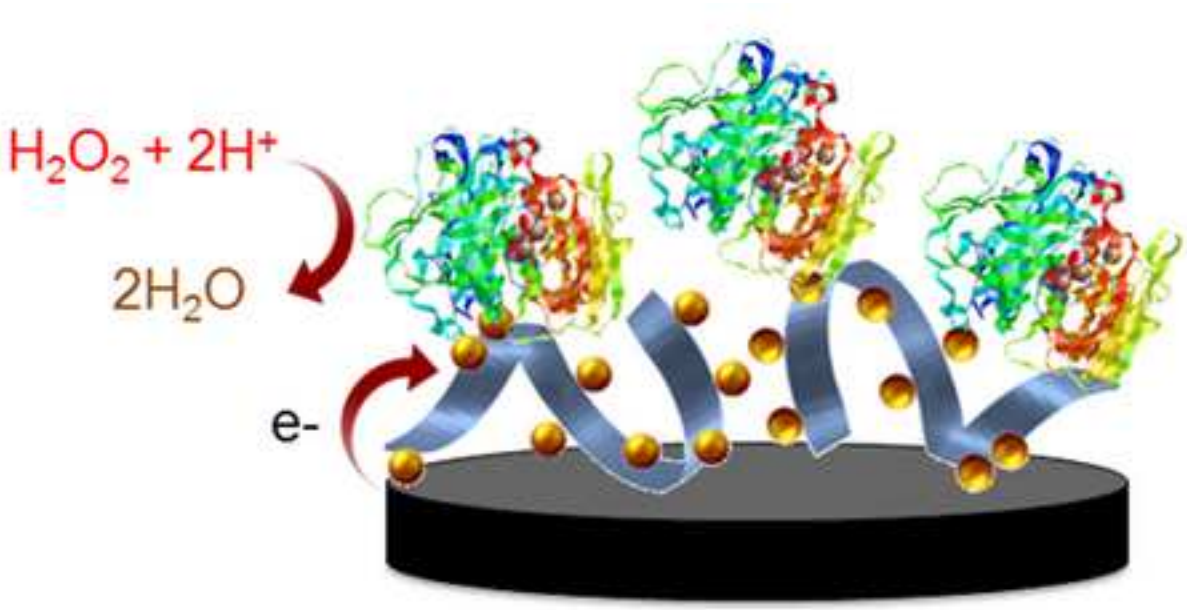

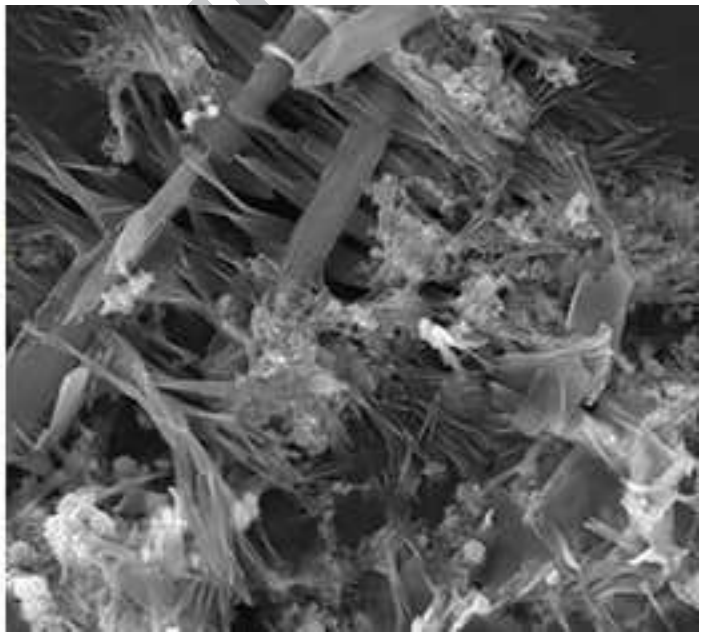

Highlights

- Novel gold nanoparticles decorated silver:bipyridine nanobelts are reported.
- Decorated nanobelts showed high electrocatalytic activity toward H2O2.
- A sensitive nanostructured enzyme biosensors for H2O2 is reported.